Combinatorial doping of TiO_2 with platinum (Pt), chromium (Cr), vanadium (V), and nickel (Ni) to achieve enhanced photocatalytic activity with visible light irradiation

Jina Choi
W.M. Keck Laboratories, California Institute of Technology, Pasadena, California 91125
Hyunwoong Park
School of Physics and Energy Science, Kyungpook National University, Daegu 702-701, South Korea
Michael R. Hoffmann[a)]
W.M. Keck Laboratories, California Institute of Technology, Pasadena, California 91125

(Received 19 May 2009; accepted 2 July 2009)

Titanium dioxide (TiO_2) was doped with the combination of several metal ions including platinum (Pt), chromium (Cr), vanadium (V), and nickel (Ni). The doped TiO_2 materials were synthesized by standard sol-gel methods with doping levels of 0.1 to 0.5 at.%. The resulting materials were characterized by x-ray diffraction (XRD), BET surface-area measurement, scanning electron microscopy (SEM), and UV-vis diffuse reflectance spectroscopy (DRS). The visible light photocatalytic activity of the codoped samples was quantified by measuring the rate of the oxidation of iodide, the rate of degradation of methylene blue (MB), and the rate of oxidation of phenol in aqueous solutions at $\lambda >$ 400 nm. 0.3 at.% Pt-Cr-TiO_2 and 0.3 at.% Cr-V-TiO_2 showed the highest visible light photocatalytic activity with respect to MB degradation and iodide oxidation, respectively. However, none of the codoped TiO_2 samples were found to have enhanced photocatalytic activity for phenol degradation when compared to their single-doped TiO_2 counterparts.

I. INTRODUCTION

Titania (TiO_2) is the most widely used photocatalyst for the purification of water, air, and other environmental applications because of its high photocatalytic activity, excellent chemical stability, relatively low price, and its lack of any known toxicity. Redox reactions of environmental interest are initiated on the TiO_2 surface with trapped electrons and holes after band gap excitation. However, because of its wide band gap energy of ~3.2 eV, TiO_2 is active only in the ultraviolet portion of the solar spectrum. As a consequence, significant efforts have been made to develop modified forms of TiO_2 that are active under visible light irradiation ($\lambda > 400$ nm). Several different strategies have been used to extend photoactivity into the visible region. They include (i) doping with anions (e.g., nitrogen,[1–3] sulfur,[4] iodine,[5–7] and fluorine[8]), (ii) doping with metal ions,[9–18] and (iii) functionalizing TiO_2 with photosensitizers that absorb visible light.[19,20]

The most actively pursued strategy has been to increase the photoactive wavelength range and to enhance the photocatalytic activity under UV irradiation by metal ion doping of TiO_2.[21–23] Numerous metal ions have been investigated as potential dopants while several metal ions such as iron,[9–11] vanadium,[12–14] chromium,[15,16] nickel,[17] and platinum[18] have been reported to show visible light photocatalytic activity.

In addition, efforts have been made to improve the visible light photocatalytic activity of TiO_2 by codoping with two metal ions.[24–28] Ahmad et al. reported that Sc and Nb codoped TiO_2 nanoparticles are relatively more photoactive for 2-chlorophenol degradation under visible light than the particles doped with Sc or Nb alone.[25] Kato and Kudo showed that TiO_2 codoped with Sb^{5+} and Cr^{3+} ions showed higher activity than TiO_2 doped only with Cr^{3+} ions alone for O_2 evolution because of the charge compensation achieved with Sb^{5+} doping.[26] Furthermore, TiO_2 codoped with Ni^{2+} and Ta^{5+} (or Ni^{2+} and Nb^{5+}) and TiO_2 codoped with Rh^{3+} and Sb^{5+} were also shown to improve photocatalytic activity for O_2 evolution under visible light irradiation.[27,28] However, there have been relatively few studies reported for double metal ion codoping of TiO_2, while TiO_2 codoped with two nonmetallic elements (e.g., N and F codoping,[29,30] N and S codoping[31,32]) or with metal ions and nonmetallic elements[33–39] (e.g., Cr and N codoping[35] Pt and N codoping,[36] V and N codoping,[37] and Bi and S codoping[38]) have been widely investigated.

To examine the efficacy of double-doping with metal ions, we have prepared codoped TiO_2 with Pt^{4+} (or Pt^{2+}),

[a)]Address all correspondence to this author.
e-mail: mrh@caltech.edu
DOI: 10.1557/JMR.2010.0024

Cr^{3+}, V^{3+}, and Ni^{2+} ions and characterized their physicochemical properties and photocatalytic activities for the bleaching and degradation of methylene blue (MB), the oxidation of iodide to tri-iodide, and the oxidative degradation of phenol in aqueous solution under visible light irradiation ($\lambda > 400$ nm).

II. EXPERIMENTAL

A. Sample preparation

TiO_2 nanoparticles were prepared by standard sol-gel methods. 5.0 mL of titanium tetraisopropoxide (TTIP, Aldrich, St. Louis, MO) was dissolved in 50 mL of absolute ethanol (Mallinckrodt, Phillipsburg, NJ) and then added dropwise to 50 mL of distilled water adjusted to pH 1.5 with nitric acid under vigorous stirring at room temperature. After 24 h, the resulting transparent colloidal suspensions were evaporated using a rotary evaporator at 45 °C and dried in the oven (70 °C) overnight. The resulting powders were calcined at 400 °C for 1 h under air. Single or double-doped TiO_2 samples (M-TiO_2 or MM-TiO_2) were prepared by adding one or two metal precursors to the distilled water prior to the hydrolysis of TTIP to give a doping level from 0.1 to 0.5 at.%. Platinum (Pt^{4+} and Pt^{2+}), chromium (Cr^{3+}), vanadium (V^{3+}), and nickel (Ni^{2+}) were selected as metal-ion dopants in this study. $PtCl_4$ (Aldrich), $Pt(NH_3)_4(NO_3)_2$ (Alfar Aesar, Ward Hill, MA), $Cr(NO_3)_3{\cdot}9H_2O$ (Aldrich), VCl_3 (Aldrich), and $Ni(NO_3)_2{\cdot}6H_2O$ (Alfar Aesar) were used as precursor reagents. Six different TiO_2 samples were synthesized and codoped with (i) Pt^{4+} and Cr^{3+} ions [Pt(IV)-Cr-TiO_2], (ii) Pt^{2+} and Cr^{3+} ions [Pt(II)-Cr-TiO_2], (iii) Cr^{3+} and V^{3+} ions (Cr-V-TiO_2), (iv) Pt^{2+} and V^{3+} ions [Pt(II)-V-TiO_2], (v) Pt^{2+} and Ni^{2+} ions [Pt(II)-Ni-TiO_2], and (vi) Cr^{3+} and Ni^{2+} ions (Cr-Ni-TiO_2). In addition, a control sample without doping was prepared along with singly-doped TiO_2 [i.e., Pt(IV)-TiO_2, Pt(II)-TiO_2, Cr-TiO_2, V-TiO_2, and Ni-TiO_2] for comparison with codoped TiO_2.

B. Characterization

We used x-ray diffraction (XRD) to examine the crystal structures of synthesized TiO_2 particles by using a Philips diffractometer (X'pert Pro) with Cu-Kα radiation. Brunauer-Emmett-Teller (BET) surface area measurement was carried out by using N_2 as the adsorptive gas (Micromeritics Gemini series, Norcross, GA). Scanning electron microscopic images (SEM, LEO 1550VP model, Peabody, MA) were taken to investigate the morphology of TiO_2 particles and analysis of elemental composition was also performed with EDS (energy dispersive x-ray spectroscopy). Diffuse reflectance UV-vis absorption spectra (DRS) of powder samples were obtained using a UV-vis spectrometer (Shimadzu UV-2101PC, Columbia, MD) equipped with a diffuse reflectance accessory.

C. Photocatalytic activity measurements

The photocatalytic activity of the synthesized TiO_2 samples was quantified with respect to the rates of photobleaching and degradation of methylene blue (MB), the rates of oxidation of iodide (I^-), and the rates of oxidative degradation of phenol (PhOH). The individual photocatalyst powders were dispersed in distilled water to give a mass concentration of 1 gL^{-1}. An aliquot of the target substrate stock solution was then added to the catalyst suspension to give the specific substrate concentration (e.g., $[MB]_0 = 10$ μM, $[I^-]_0 = 50$ mM, and $[PhOH]_0 = 50$ μM). The reaction suspension pH was circum-neutral. Before irradiation, the suspension was stirred in the dark for 30 min to obtain a state of sorption equilibrium of the specific substrate on TiO_2.

A high-pressure Hg(Xe) arc lamp (500 W) was used as the light source. The light beam emitted from the arc lamp was passed through an IR water filter and a UV cut-off filter ($\lambda > 400$ nm) before being focused onto a cylindrical Pyrex reactor through a quartz window. The reactor was open to ambient air during most experiments. Time-sequenced sample aliquots were collected from the reactor during the illumination for analysis and filtered through a 0.45 μm PTFE syringe filter to remove the TiO_2 particles. Multiple photolysis (and photocatalysis) experiments were performed under identical reaction conditions to determine reproducibility.

The degradation rates and rate constants for MB loss during photocatalysis were determined by measuring the absorbance of MB at 665 nm with a spectrophotometer (Shimadzu UV-2101PC). For the photocatalytic oxidation of I^-, tri-iodide (I_3^-), which is the principal product of I^- oxidation in the presence of excess iodide ion, was spectrophotometrically determined by measuring the absorbance at 352 nm. The degradation of phenol in aqueous solution was measured using high-performance liquid chromatography (HPLC, Agilent HP 1100 series with C18 column, Santa Clara, CA).

III. RESULTS AND DISCUSSION

A. Characterization of single metal doped TiO_2 (M-TiO_2)

Singly-doped TiO_2 (M-TiO_2) samples were prepared by sol-gel synthesis where M = Pt^{4+}, Cr^{3+}, V^{3+}, and Ni^{2+}. To compare the effect of oxidation state of Pt dopant, TiO_2 doped with Pt^{2+} ions was also prepared. Figure 1 shows the XRD patterns of the singly-doped M-TiO_2 samples at the doping level of 0.3 at.%. The XRD patterns are consistent with the standard crystal structure of TiO_2 (i.e., a mixture of anatase and rutile phases) with no diffraction peaks associated with any of the doped metal elements in the M-TiO_2 samples. This indicates that the doping process does not induce the formation of separate impurity

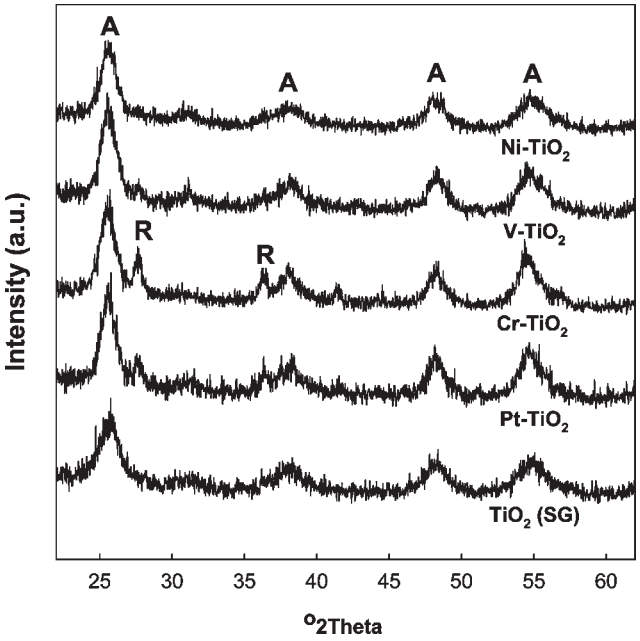

FIG. 1. X-ray diffraction (XRD) pattern measured for 0.3 at.% M-TiO_2 prepared at 400 °C (A: anatase phase, R: rutile phase).

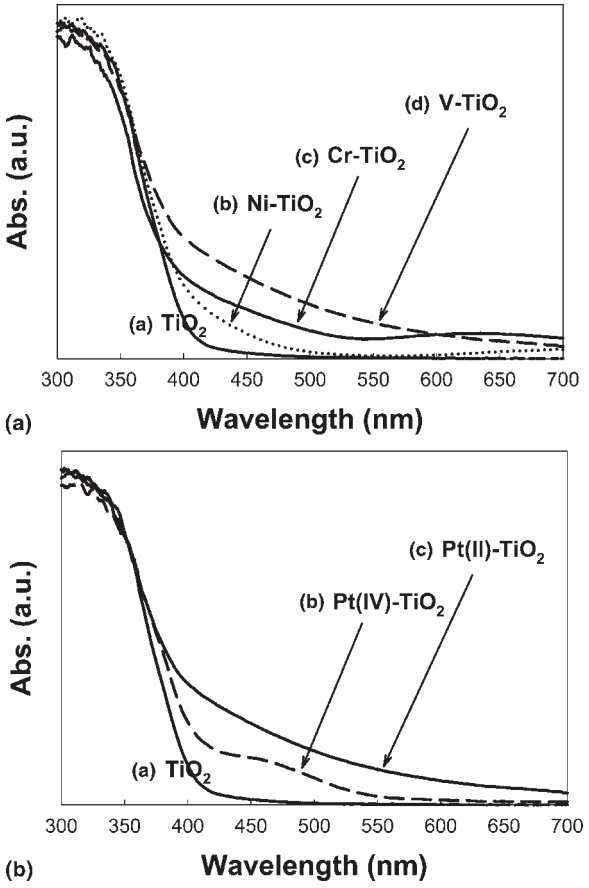

FIG. 2. UV/vis diffuse reflectance spectra (DRS) for 0.3 at.% M-TiO_2 samples: (a) undoped TiO_2, Cr-TiO_2, Ni-TiO_2, and V-TiO_2. (b) Pt(IV)-TiO_2 and Pt(II)-TiO_2.

phases and that the specific dopant could be considered to be fully incorporated into the TiO_2 lattice. Pt^{4+}, Cr^{3+}, and V^{3+} ions may be substituted into the Ti site of TiO_2 because the ionic radii of the dopants (Pt^{4+}: 0.765 Å, Cr^{3+}: 0.755 Å, and V^{3+}: 0.78 Å)[40] are similar to that of Ti^{4+} (0.745 Å).[40] However, Ni^{2+} and Pt^{2+} ions are possibly located in the interstitial position of the lattice rather than the Ti site because of the relatively large size difference between the dopant ions (Ni^{2+}: 0.83 Å and Pt^{2+}: 0.94 Å)[40] and the Ti^{4+} ions. Undoped TiO_2 samples prepared by sol-gel synthesis and calcined at 400 °C (TiO_2-SG) show only the pure anatase phase. However, the rutile phase is apparent in some M-TiO_2 samples prepared and treated at the same temperature. This result suggests that metal-ion doping lowers the relative temperature of the anatase-to-rutile phase transformation (A-R phase transformation). 0.3 at.% Cr-TiO_2 and 0.3 at.% Pt-TiO_2 [both Pt(IV)-TiO_2 and Pt(II)-TiO_2] exhibit a characteristic rutile peak whereas 0.3 at.% V-TiO_2 appear to have a smaller fraction of the rutile phase. 0.3 at.% Ni-TiO_2, by contrast, shows a pure anatase phase as in the case of undoped TiO_2. Therefore, we conclude that doping TiO_2 with Cr, Pt, and V ions modifies the temperature dependence of the A-R phase transformation.

Figure 2 shows the UV/vis diffuse reflectance spectra for the various M-TiO_2 samples. Undoped TiO_2 exhibits a sharp absorption edge at about 400 nm ($E_{bg} \approx 3.1$ eV). However, the M-TiO_2 samples show absorption spectra extended into the visible region over the range of 400–700 nm. Thus, visible light activation and photocatalytic activity could be expected from these M-TiO_2 samples. As shown in Fig. 2(a), 0.3 at.% Ni-TiO_2 gives a relatively small absorption between 400 and 500 nm while 0.3 at.% V-TiO_2 exhibits a more substantial and broader absorption shoulder up to 700 nm. 0.3 at.% Cr-TiO_2 also shows extended absorption spectra over the 400–500 nm range with an additional absorption peak near 650 nm; this may be due to the *d-d* transitions of Cr^{3+} ions.[26,41] Figure 2(b) shows the difference between the absorption spectra of 0.3 at.% Pt(IV)-TiO_2 and 0.3 at.% Pt(II)-TiO_2. Pt(II)-TiO_2 gives a broad absorption over most of the visible region similar to 0.3 at.% V-TiO_2. In contrast, 0.3 at.% Pt(IV)-TiO_2 gives a smaller absorption peak between 400 and 550 nm; this indicates that the origins of the absorption spectra are different in the two different Pt-TiO_2 samples. The extended absorption of the M-TiO_2 into the visible region has been explained in terms of the excitation of electrons of the dopant ion to the TiO_2 conduction band (i.e., a metal to conduction band charge transfer) according to their respective energy levels.[12,13,42,43] However, recent proposals suggest that the absorption spectra of modified TiO_2 in the visible region most likely originate from defects associated with oxygen vacancies that give rise to colored

centers.[44,45] Kuznetsov and Serpone pointed out the similarities of the spectra in the range of 400–600 nm shown among different types of visible light active TiO_2 samples.[44] It was also reported that similar absorption spectra in the visible region are found in reduced TiO_2 samples with observed absorption spectra being the sum of overlapping absorption bands with the maxima at 2.81 eV and 2.55 eV, which correlate with oxygen vacancies.[46,47] The metal-ion dopants used in this study have different valence states than Ti^{4+}, and as a consequence, may induce the generation of oxygen vacancies during synthesis. In addition, some of the M-TiO_2 samples [e.g., Ni-TiO_2, V-TiO_2, Pt(II)-TiO_2] exhibit similar absorption in the range of 400–600 nm, even though the absorption intensities are different. Therefore, both the generation of new energy levels due to the injection of impurities within the band gap energies range and the generation of oxygen vacancies by metal doping may contribute to the observed visible light absorption of M-TiO_2 samples.

B. Characterization of metal codoped TiO_2 (MM-TiO_2)

The properties of 0.3 at.% MM-TiO_2 samples are summarized in Table I. The doubly-doped MM-TiO_2 samples exhibit a variety of colors; TiO_2 samples doped with Cr or Ni are green; Pt doped samples are brown; and V doped samples are orange. The BET surface area of the sol-gel synthesized, undoped TiO_2, which was calcined at 400 °C, is 104 cm^2/g whereas the surface area of the Degussa P25 TiO_2 is 50 cm^2/g, indicating that the TiO_2 particles synthesized by sol-gel methods have substantially higher surface areas and adsorption capacities per unit weight than Degussa P25. The surface areas of 0.3 at.% M-TiO_2 samples are slightly larger than the undoped TiO_2 (106–132 cm^2/g). However, there are no significant increases in the surface areas of doubly-doped samples ($\sim$110 cm^2/g).

TABLE I. Characterization of MM-TiO_2 photocatalysts at 0.3 at.% doping level.

Sample	Color	Surface area (m^2g^{-1})	Crystal structure (X_R %)
TiO_2 (SG)	White	104	Anatase (0)
Pt(II)-TiO_2	Light brown	111	Anatase/Rutile (22)
Pt(IV)-TiO_2	Light brown	106	Anatase/Rutile (26)
Cr-TiO_2	Green	115	Anatase/Rutile (34)
V-TiO_2	Orange	132	Anatase/Rutile (13)
Ni-TiO_2	Green	112	Anatase (0)
Pt(II)-Cr-TiO_2	Dark green	112	Anatase/Rutile (30)
Pt(IV)-Cr-TiO_2	Dark green	108	Anatase/Rutile (32)
Cr-V-TiO_2	Brown	115	Anatase/Rutile (28)
Pt(II)-V-TiO_2	Brown	118	Anatase/Rutile (24)
Pt(II)-Ni-TiO_2	Light green	110	Anatase (0)
Cr-Ni-TiO_2	Green	115	Anatase (0)

XRD patterns of 0.3 at.% Pt(IV)-0.3 at.% Cr-TiO_2 and 0.3 at.% Cr-0.3 at.% Ni-TiO_2 are shown in Fig. 3 with XRD patterns of each singly-doped TiO_2. Crystal structures of all MM-TiO_2 samples are also listed in Table I along with the BET surface areas. Figure 3(a) shows that a rutile phase of Cr or Pt singly-doped TiO_2 was well maintained in doubly-doped Pt(IV)-Cr-TiO_2 samples. In Fig. 3(b), however, the 0.3 at.% Cr-0.3 at.% Ni-TiO_2 sample appears to lack evidence for a rutile phase that was clearly shown in singly-doped 0.3 at.% Cr-TiO_2. Similarly, 0.3 at.% Pt(II)-0.3 at.% Ni-TiO_2 appears to be a pure anatase phase material despite 0.3 at.% Pt(II) doping. Therefore, we suggest that codoping with Ni ions may inhibit the A-R phase transformation in Cr-TiO_2 or Pt-TiO_2.

For comparison, the fraction of rutile, X_R, as calculated from the respective peak intensities using the following equation[48]:

$$X_R(\%) = \{1 - (1 + 1.26I_R/I_A)^{-1}\} \times 100$$

where I_R and I_A are the x-ray intensities of the rutile (101) and anatase (110) peaks, respectively. These relative rutile fractions are listed in Table I. These results

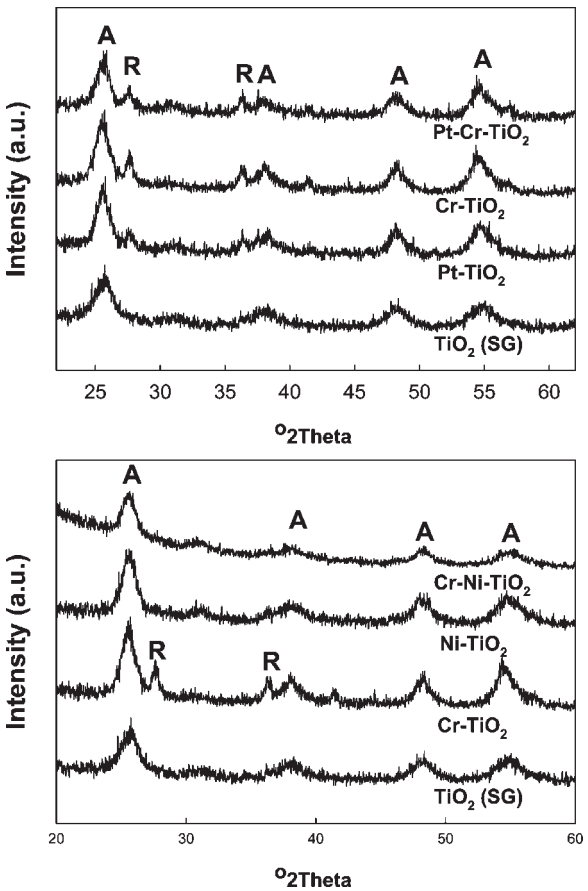

FIG. 3. X-ray diffraction (XRD) pattern measured for 0.3 at.% Pt-Cr-TiO_2 and Cr-Ni-TiO_2 (A: anatase phase, R: rutile phase).

show that the fraction of rutile (X_R) in MM-TiO_2 is not higher than that for each of the M-TiO_2 samples. For example, X_R of 0.3 at.% Pt(IV)-Cr-TiO_2 is estimated to be 32%, while X_R of 0.3 at.% Pt(IV)-TiO_2 and 0.3 at.% Cr-TiO_2 are estimated as 26% and 34%, respectively. Furthermore, 0.3 at.% Pt(II)-0.3 at.% V-TiO_2 and 0.3 at.% Cr-0.3 at.% V-TiO_2 have similar or smaller X_R values than those of 0.3 at.% Pt(II)-TiO_2, 0.3 at.% V-TiO_2, or 0.3 at.% Cr-TiO_2.

Figure 4 shows SEM images of 0.3 at.% Pt-0.3 at.% Cr-TiO_2. In Fig. 4(a), 0.3 at.% Pt(IV)-0.3 at.% Cr-TiO_2 particles are aggregated together and show rough morphologies. 0.3 at.% Pt(II)-0.3 at.% Cr-TiO_2 [Fig. 4(b)] and other MM-TiO_2 (images not shown here) also show SEM images similar to 0.3 at.% Pt(IV)-0.3 at.% Cr-TiO_2. Niishiro et al. reported that doping with Sb^{3+} ions in TiO_2 suppressed sintering due to the difference in size between Sb^{3+} (0.90 Å) and Ti^{4+}, which results in the formation of finer and smoother crystalline particles.[28] However, in our case, the doping of 0.3 at.% Pt^{2+} (0.94 Å) does not significantly change either the size of particle or the morphology [Fig. 4(b)]. This may be due to the relatively low doping level (0.3% versus 0.5–2%) and a lower calcination temperature (400 °C versus 1150 °C). In addition, the EDS spectrum of 0.3 at.% Pt(II)-0.3 at.% Ni-TiO_2 [Fig. 4(c)] shows no apparent signals for Pt and Ni; only those of Ti and O are observed. This indicates that metal ions with larger ionic radii than Ti^{4+} such as Pt^{2+} or Ni^{2+} ions are well incorporated into the TiO_2 lattice and not located in the surface region; these results are consistent with XRD results.

There are no significant differences between 0.3 at.% Pt(IV)-0.3 at.% Cr-TiO_2 and 0.3 at.% Pt(II)-0.3 at.% Cr-TiO_2 in terms of the XRD pattern, BET surface areas, morphology, and element analysis as determined by EDS. However, UV/vis DRS results clearly show the difference between two samples as shown in Fig. 5. 0.3 at.% Pt(IV)-0.3 at.% Cr-TiO_2 shows an enhanced absorption compared to 0.3 at.% Pt-TiO_2 or 0.3 at.% Cr-TiO_2. The spectral response of 0.3 at.% Pt(IV)-0.3 at.% Cr-TiO_2 appears to be an addition spectrum of the singly-doped 0.3 at.% Pt-TiO_2 combined with that of 0.3 at.% Cr-TiO_2 [Fig. 5(a)]. On the other hand, the absorption of 0.3 at.% Pt(II)-0.3 at.% Cr-TiO_2 is almost identical to 0.3 at.% Cr-TiO_2 [Fig. 5(b)]. Therefore, we expect that absorption of visible light is more efficient in the 0.3 at.% Pt(IV)-0.3 at.%

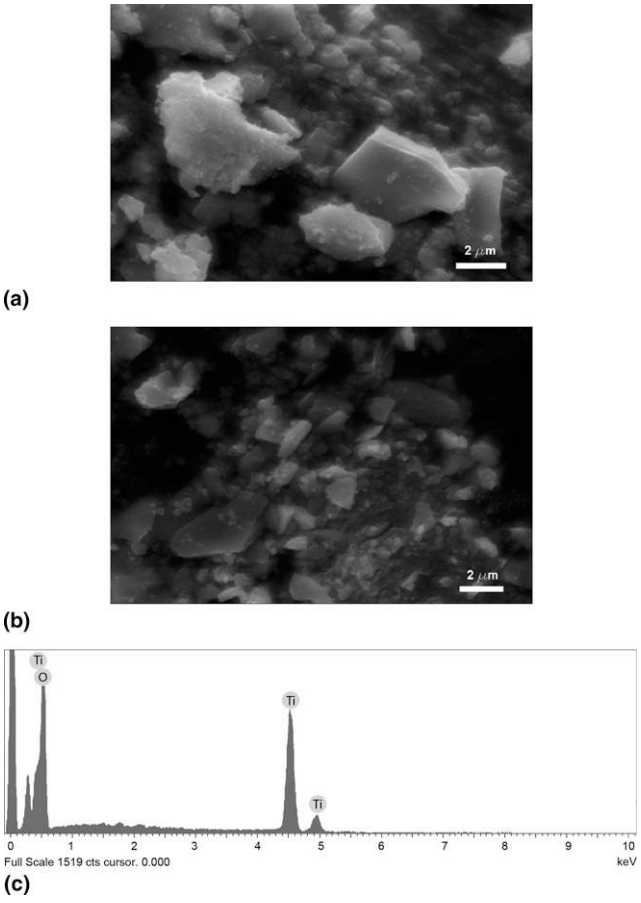

FIG. 4. SEM images of (a) 0.3 at.% Pt(IV)-Cr-TiO_2 and (b) 0.3 at.% Pt(II)-Cr-TiO_2, and (c) EDS spectra of Pt(II)-Ni-TiO_2 that clearly shows dopants signals (i.e., Pt and Ni) other than Ti and O signals were not observed.

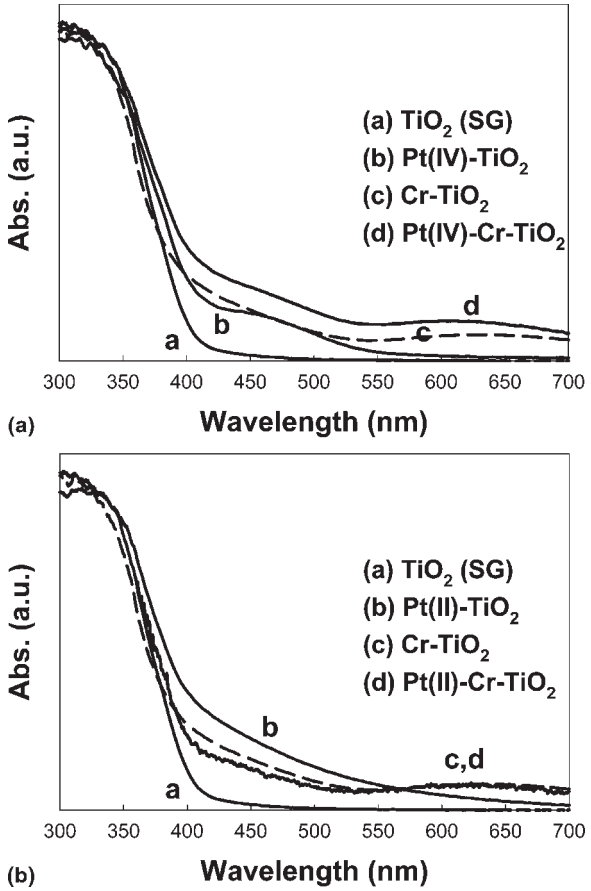

FIG. 5. UV/vis diffuse reflectance spectra (DRS) for 0.3 at.% Pt-Cr-TiO_2: (a) Pt(IV)-Cr-TiO_2, (b) Pt(II)-Cr-TiO_2 samples.

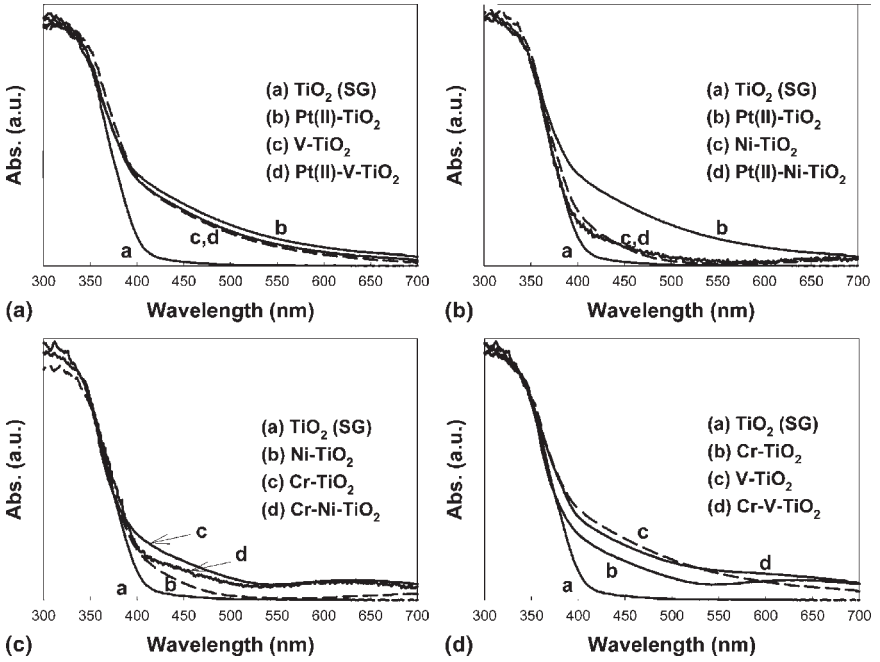

FIG. 6. UV/vis diffuse reflectance spectra (DRS) for (a) 0.3 at.% Pt(II)-V-TiO_2, (b) 0.3 at.% Pt(II)-Ni-TiO_2, (c) 0.3 at.% Cr-Ni-TiO_2, and (d) 0.3 at.% Cr-V-TiO_2.

Cr-TiO_2 samples than the singly-doped 0.3 at.% Pt(IV)-TiO_2 samples.

Figure 6 shows UV/vis DRS results for other doubly-doped MM-TiO_2 materials. The absorption spectra of the 0.3 at.% Pt(II)-0.3 at.% V-TiO_2 sample [Fig. 6(a)] and the 0.3 at.% Pt(II)-0.3 at.% Ni-TiO_2 sample [Fig. 6(b)] were the same as those of 0.3 at.% singly-doped V-TiO_2 and Ni-TiO_2 samples, respectively. In all the cases of Pt(II)-M-TiO_2, the Pt(II) is not attributed to the absorption spectra of the codoped TiO_2. In contrast, Pt(IV) is the only effective codopant for enhanced visible light absorption in the Cr-M-TiO_2 samples. For example, 0.3 at.% Cr-0.3 at.% Ni-TiO_2 [Fig. 6(c)] and 0.3 at.% Cr-0.3 at.% V-TiO_2 [Fig. 6(d)] does not show enhanced absorption compared to the sum of singly-doped TiO_2, while 0.3 at.% Cr-0.3 at.% Pt(IV)-TiO_2 has a significantly enhanced absorption in the visible region [Fig. 5(a)].

C. Visible light photocatalytic activity

Figure 7 shows visible light photocatalytic activities of various M-TiO_2 and MM-TiO_2 preparations for the degradation of methylene blue (MB) in aqueous solution. The degradation and bleaching reaction follow apparent first-order kinetics. Under visible light irradiation at $\lambda > 400$ nm, direct photolysis of MB is observed in the absence of TiO_2 particles since MB molecules can absorb visible light and become photolyzed without the photocatalyst. The measured first-order rate constant, k_{MB}, increases slightly in the presence of undoped TiO_2. This increase may be due to additional light absorption above 400 nm by the TiO_2 particles or by an enhanced electron transfer from MB to the conduction band of TiO_2. All the singly-doped M-TiO_2 preparations show visible light photocatalytic activity for MB degradation while the 0.3 at.% Pt(II)-TiO_2 samples give the highest values for k_{MB}. Among doubly-doped MM-TiO_2 samples, only 0.3 at.% Pt-0.3 at.% Cr-TiO_2 [both Pt(IV) and Pt(II)] and Pt(II)-Ni-TiO_2 show higher k_{MB} values than those measured for the singly-doped TiO_2 samples. Therefore, codoping with Pt appears to be effective for enhancing the visible light degradation of MB degradation. On the other hand, the doubly-doped Pt-V-TiO_2 samples have lower photocatalytic activity, which may be due to the effect of V doping.

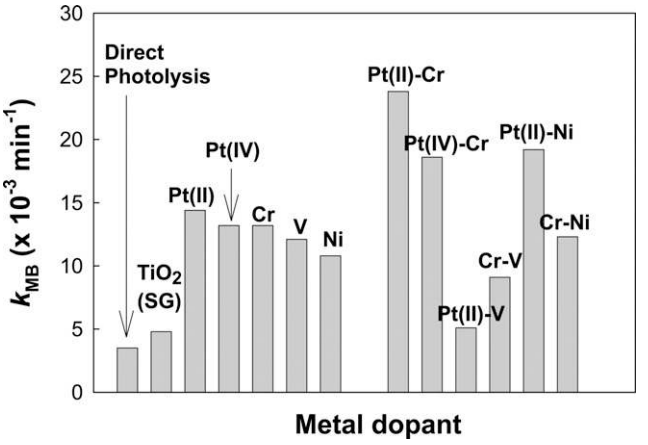

FIG. 7. The comparison of degradation rate constant (k_{MB}) of MB for various single-doped or codoped TiO_2 samples (0.3 at.% doping).

0.3 at.% Pt(IV)-0.3 at.% Cr-TiO_2, which has enhanced visible light absorption [Fig. 5(a)], is less photoactive than 0.3 at.% Pt(II)-0.3 at.% Cr-TiO_2. Conversely, 0.3 at.% Cr-0.3 at.% V-TiO_2 and 0.3 at.% Pt(II)-0.3 at.% V-TiO_2 have significantly decreased k_{MB} values compared to their singly-doped TiO_2 counterparts. In comparison to the 0.3 at.% Cr-0.3 at.% Ni-TiO_2 and 0.3 at.% Pt(II)-0.3 at.% Ni-TiO_2 samples, V codoping of Cr-TiO_2 and Pt-TiO_2 show a net negative effect on photocatalytic activity. However, these samples still show better photocatalytic activity than undoped TiO_2.

The photocatalytic oxidation of iodide ions (I^-) can also be used to compare the visible light photocatalytic activities of various MM-TiO_2 preparations. Iodide in aqueous solution is readily oxidized to tri-iodide (I_3^-) according to the following reaction:

$$I^- + h_{vb}^+ \longrightarrow I^{\cdot} \xrightarrow{+I^{\cdot}} I_2 \xrightarrow{+I^-} I_3^- \quad .$$

Figure 8 shows the production of I_3^- ions from I^- oxidation under visible light irradiation in the presence of doubly-doped MM-TiO_2 materials. As a control measurement, no I_3^- is produced in the absence of TiO_2 particles at $\lambda > 400$ nm. Undoped TiO_2, 0.3 at.% V-TiO_2, and 0.3 at.% Pt(II)-TiO_2 show little photocatalytic activity with respect to the net photooxidation of I^- to I_3^-. However, 0.3 at.% V-0.3 at.% Cr-TiO_2 and 0.3 at.% Pt(II)-0.3 at.% Cr-TiO_2 have higher photoactivity. Therefore, Cr is clearly an effective codopant with respect to I^- photooxidation in the visible spectrum. I_3^- production is very fast during the initial phases of the reaction, but it slows noticeably as irradiation continues. This is due to the back photoreaction of I_3^- with conduction-band electrons to reform I^- ions. The back reaction effectively competes with the forward reaction of iodide with valence-band holes or surface hydroxyl radicals as the concentration of I_3^- increases with time.

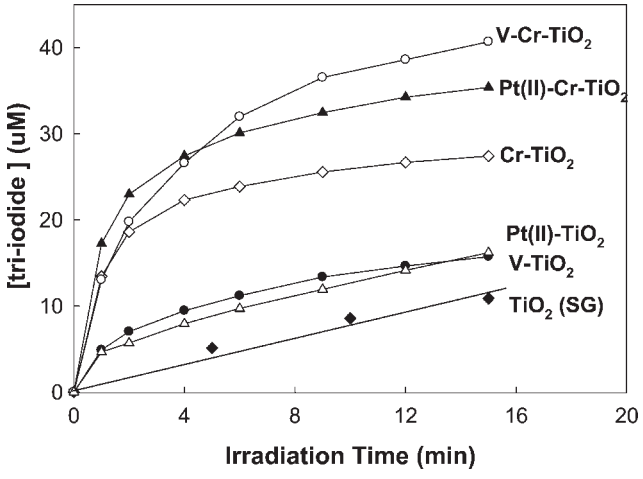

FIG. 8. The production of tri-iodide by iodide oxidation ($[I^-]_0$ = 50 mM, total volume = 30 mL) with selected MM-TiO_2 (0.3 at.% doping level, 1 g/L) under visible light irradiation (500 W, >400 nm).

In Fig. 9, the photocatalytic activity of the singly-doped M-TiO_2 samples and the doubly-doped MM-TiO_2 samples are compared in terms of total amount of I_3^- ions produced during 15 min of irradiation. Similar to MB degradation, all the M-TiO_2 samples improve the I^- oxidation rates; 0.3 at.% Pt(IV)-TiO_2 and 0.3 at.% Cr-TiO_2 show the highest activity. However, 0.3 at.% Pt(II)-TiO_2, 0.3 at.% V-TiO_2, and 0.3 at.% Ni-TiO_2, which have comparable activities to 0.3 at.% Pt(IV)-TiO_2 or 0.3 at.% Cr-TiO_2 in terms of MB degradation, show only slightly enhanced I^- oxidation rates. Most of the MM-TiO_2 samples also show some enhanced photocatalytic activity. 0.3 at.% Pt(II)-0.3 at.% V-TiO_2 has the least visible light activity among the doubly-doped MM-TiO_2 samples.

The doping level of each dopant in Pt(II)-Cr-TiO_2 is also optimized. Table II shows photocatalytic activities of Pt(II)-Cr-TiO_2 with different concentrations of Pt and Cr over the range of 0.1–0.5 at.%. The optimal concentration for increased photocatalytic activity is 0.3 at.% Pt(II) and 0.3 at.% Cr. It is also observed that photocatalytic activity with respect to I^- oxidation strongly depends on Cr concentration.

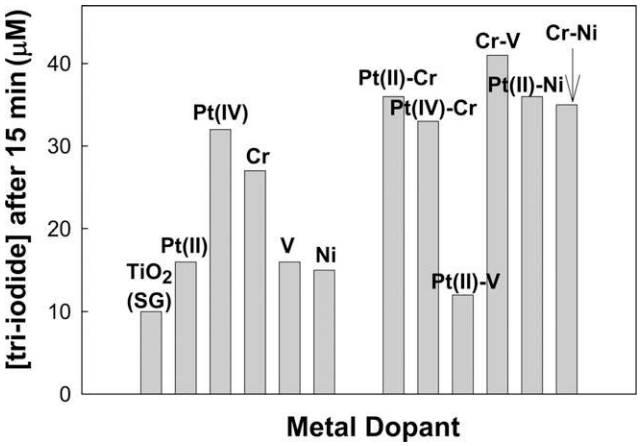

FIG. 9. The comparison of various single-doped or co-doped TiO_2 samples (0.3 at.% doping) for I^- oxidation.

TABLE II. Photocatalytic activities of Pt(II)-Cr-TiO_2 with different doping level for I oxidation under visible-light irradiation (>400 nm).

Sample	$[I^{3-}]$produced (μM) after 15 min
0.3% Pt(II) with	
0% Cr	16
0.1% Cr	19
0.2% Cr	21
0.3% Cr	36
0.5% Cr	32
0.3% Cr with	
0% Pt	29
0.1% Pt	31
0.2% Pt	28
0.3% Pt	36
0.5% Pt	32

The photocatalytic degradation of phenol under visible light irradiation is shown in Fig. 10. Phenol is degraded effectively with Pt-TiO_2 [both Pt(IV)-TiO_2 and Pt(II)-TiO_2] and totally degraded within 2 h with 0.3 at.% Pt(IV)-TiO_2. However, 0.3 at.% Pt-0.3 at.% Cr-TiO_2 does not exhibit any enhancement in the photodegradation of phenol [Fig. 10(a)]. Phenol degradation with 0.3 at.% Pt(IV)-TiO_2 is slightly decreased by Cr codoping. Moreover, the resultant photocatalytic activity of 0.3 at.% Pt(II)-0.3 at.% Cr-TiO_2 is much less than 0.3 at.% Pt(II)-TiO_2. Similarly, there is no advantage shown by the doubly-doped Cr-V-TiO_2 samples [Fig. 10(b)]. The other doubly-doped MM-TiO_2 samples, which are not shown here, also have negative codoping effects with respect to phenol degradation. These results clearly indicate that the codoping effects on TiO_2 photocatalytic activity are substrate-dependent. Several doubly-doped MM-TiO_2 samples show enhanced photocatalytic activity for MB degradation or I^- oxidation. For example, 0.3 at.% Pt(II)-0.3 at.% Cr-TiO_2 and 0.3 at.% Cr-0.3 at.% V-TiO_2 show the highest visible light photocatalytic activity for MB degradation and I^- oxidation, respectively. However, there is no apparent enhancement observed for doubly-doped TiO_2 materials for phenol photodegradation.

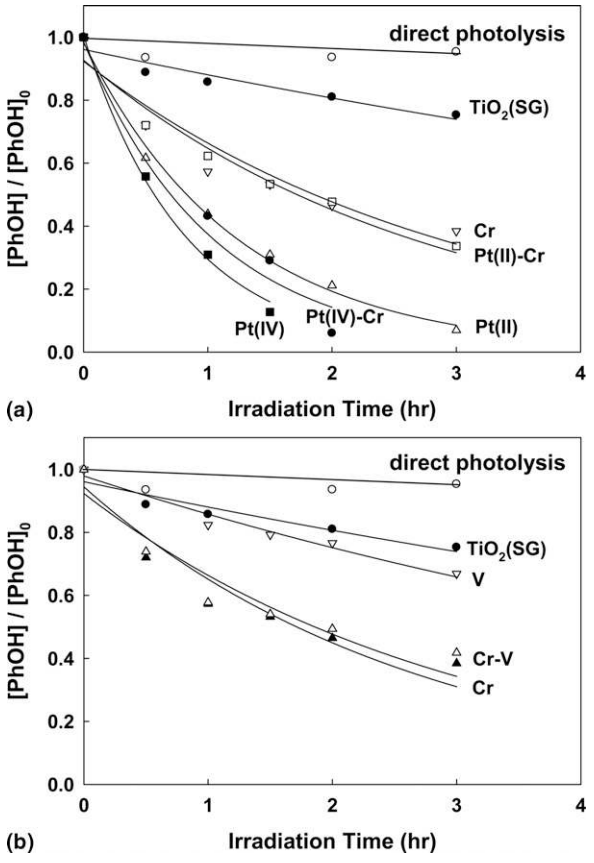

FIG. 10. The degradation of phenol ([phenol]$_0$ = 50 μM, 1 g/L of 0.3 at.% single-doped or codoped TiO_2, >400 nm): (a) Pt-Cr-TiO_2, (b) Cr-V-TiO_2.

It is worth mentioning that photocatalytic activities of MM-TiO_2 were observed substrate-dependent and are not correlated with any physicochemical property of MM-TiO_2. Neither the absorption spectra in the visible region nor the crystal structures (anatase and rutile) of MM-TiO_2 appear to play an important role in the visible light induced photocatalytic reactions. For example, Pt(IV)-Cr-TiO_2, which was expected to have more efficient absorption of visible light than Pt(II)-Cr-TiO_2, shows less photocatalytic activity than Pt(II)-Cr-TiO_2 for both MB degradation and I^- oxidation. However, Pt(IV)-Cr-TiO_2 shows higher photocatalytic activity than Pt(II)-Cr-TiO_2 for phenol degradation. In addition, Pt(II)-V-TiO_2 that has larger visible light absorption than Pt(II)-Ni-TiO_2 is less photoactive for MB degradation and I^- oxidation, as well. Similarly, the structure (i.e., the fraction of rutile) in MM-TiO_2 does not affect the visible light photocatalytic activity of MM-TiO_2. Pt(IV)-Cr-TiO_2 with a high relative rutile content and Pt(II)-Ni-TiO_2 with no rutile at all show comparable photocatalytic activity for MB degradation. For I^- oxidation, Pt(II)-Ni-TiO_2 and Cr-Ni-TiO_2 also show comparable photocatalytic activity to Pt(II)-Cr-TiO_2.

IV. CONCLUSION

TiO_2 codoped with two metal ions was prepared by adding Pt (Pt^{4+} and Pt^{2+}), Cr^{3+}, V^{3+}, and Ni^{2+} ions during sol-gel synthesis. The metal ion dopants used in this study are effectively incorporated into the TiO_2 lattice either in Ti(IV) sites or in interstitial sites. Single and double ion doping changes some of the physicochemical properties such as the reactive surface area and photophysical response of pristine TiO_2. 0.3 at.% Pt-0.3 at.% Cr-TiO_2 (both Pt^{4+} and Pt^{2+}), 0.3 at.% Cr-0.3 at.% V-TiO_2, and 0.3 at.% Pt-0.3 at.% V-TiO_2 samples lower the A-R phase-transformation temperature since an individual dopant used for codoping also has an enhancing effect on A-R phase transformation. However, 0.3 at.% Pt-0.3 at.% Ni-TiO_2 and 0.3 at.% Cr-0.3 at.% Ni-TiO_2 remain strictly in the anatase phase due to Ni codoping although doping with Pt and Cr alone accelerate A-R phase transformation. All codoped TiO_2 materials give extended UV-vis absorption between 400 and 700 nm, but only 0.3 at.% Pt (IV)-0.3 at.% Cr-TiO_2 enhanced visible light absorption compared to singly-doped TiO_2. Visible light photocatalytic activities are evaluated for the degradation of MB, phenol, and the oxidation of I^- in aqueous solution. The photocatalytic activities of codoped TiO_2 strongly depends on the nature of the electron-donating substrate and are not correlated with any physicochemical property of the codoped TiO_2. Pt-Cr-TiO_2 and Pt-Ni-TiO_2 enhance the rate of MB degradation while Pt-Cr-TiO_2, Cr-V-TiO_2, Pt-Ni-TiO_2, and Cr-Ni-TiO_2 show enhanced activity for I^- oxidation. However, none of the codoped samples

show enhanced photocatalytic activity for phenol degradation compared to their singly-doped TiO_2 counterparts. All codoped TiO_2 samples exhibit some enhancement in photocatalytic activity for all three reactions compared to undoped nanoparticulate TiO_2.

ACKNOWLEDGMENTS

We gratefully acknowledge the generous support for this research that has been provided by the Northrop-Grumman Corporation. In particular, we would like to give special credit to Dr. Ronald Pirich for his enthusiastic encouragement and intellectual support for our joint projects over the years.

REFERENCES

1. R. Asahi, T. Morikawa, T. Ohwaki, K. Aoki, and Y. Taga: Visible-light photocatalysis in nitrogen-doped titanium oxides. *Science* **293,** 269 (2001).
2. M. Mrowetz, W. Balcerski, A.J. Colussi, and M.R. Hoffman: Oxidative power of nitrogen-doped TiO_2 photocatalysts under visible illumination. *J. Phys. Chem. B* **108,** 17269 (2004).
3. G. Sauthier, E. Gyorgy, and A. Figueras: Investigation of nitrogen-doped TiO_2 thin films grown by reactive pulsed laser deposition. *J. Mater. Res.* **23,** 2340 (2008).
4. T. Umebayashi, T. Yamaki, S. Tanaka, and K. Asai: Visible light-induced degradation of methylene blue on S-doped TiO_2. *Chem. Lett.* **32,** 330 (2003).
5. W.Y. Su, Y.F. Zhang, Z.H. Li, L. Wu, X.X. Wang, J.Q. Li, and X.Z. Fu: Multivalency iodine doped TiO_2: Preparation, characterization, theoretical studies, and visible-light photocatalysis. *Langmuir* **24,** 3422 (2008).
6. G. Liu, Z.G. Chen, C.L. Dong, Y.N. Zhao, F. Li, G.Q. Lu, and H.M. Cheng: Visible light photocatalyst: Iodine-doped mesoporous titania with a bicrystalline framework. *J. Phys. Chem. B* **110,** 20823 (2006).
7. X.T. Hong, Z.P. Wang, W.M. Cai, F. Lu, J. Zhang, Y.Z. Yang, N. Ma, and Y.J. Liu: Visible-light-activated nanoparticle photocatalyst of iodine-doped titanium dioxide. *Chem. Mater.* **17,** 1548 (2005).
8. J.K. Zhou, L. Lv, J.Q. Yu, H.L. Li, P.Z. Guo, H. Sun, and X.S. Zhao: Synthesis of self-organized polycrystalline F-doped TiO_2 hollow microspheres and their photocatalytic activity under visible light. *J. Phys. Chem. C* **112,** 5316 (2008).
9. X.W. Zhang and L.C. Lei: One step preparation of visible-light responsive Fe-TiO_2 coating photocatalysts by MOCVD. *Mater. Lett.* **62,** 895 (2008).
10. X.W. Zhang, M.H. Zhou, and L.C. Lei: Co-deposition of photocatalytic Fe doped TiO_2 coatings by MOCVD. *Catal. Commun.* **7,** 427 (2006).
11. W.Y. Teoh, R. Amal, L. Madler, and S.E. Pratsinis: Flame sprayed visible light-active Fe-TiO_2 for photomineralisation of oxalic acid. *Catal. Today* **120,** 203 (2007).
12. K. Iketani, R.D. Sun, M. Toki, K. Hirota, and O. Yamaguchi: Sol-gel-derived $V_xTi_{1-x}O_2$ films and their photocatalytic activities under visible light irradiation. *Mater. Sci. Eng., B* **108,** 187 (2004).
13. S. Klosek and D. Raftery: Visible light driven V-doped TiO_2 photocatalyst and its photooxidation of ethanol. *J. Phys. Chem. B* **105,** 2815 (2001).
14. J.C.S. Wu and C.H. Chen: A visible-light response vanadium-doped titania nanocatalyst by sol-gel method. *J. Photochem. Photobiol., A* **163,** 509 (2004).
15. E. Borgarello, J. Kiwi, M. Gratzel, E. Pelizzetti, and M. Visca: Visible-light induced water cleavage in colloidal solutions of chromium-doped titanium-dioxide particles. *J. Am. Chem. Soc.* **104,** 2996 (1982).
16. M. Anpo, Y. Ichihashi, M. Takeuchi, and H. Yamashita: Design and development of unique titanium oxide photocatalysts capable of operating under visible light irradiation by an advanced metal ion-implantation method. *Sci. Technol. Catal.* **121,** 305 (1999).
17. D.H. Kim, K.S. Lee, Y.S. Kim, Y.C. Chung, and S.J. Kim: Photocatalytic activity of Ni 8 wt%-doped TiO_2 photocatalyst synthesized by mechanical alloying under visible light. *J. Am. Ceram. Soc.* **89,** 515 (2006).
18. S. Kim, S.J. Hwang, and W.Y. Choi: Visible light active platinum-ion-doped TiO_2 photocatalyst. *J. Phys. Chem. B* **109,** 24260 (2005).
19. H. Park, W. Choi, and M.R. Hoffmann: Effects of the preparation method of the ternary CdS/TiO_2/Pt hybrid photocatalysts on visible light-induced hydrogen production. *J. Mater. Chem.* **18,** 2379 (2008).
20. E. Bae and W. Choi: Highly enhanced photoreductive degradation of perchlorinated compounds on dye-sensitized metal/TiO_2 under visible light. *Environ. Sci. Technol.* **37,** 147 (2003).
21. W.Y. Choi, A. Termin, and M.R. Hoffmann: The role of metal-ion dopants in quantum-sized TiO_2—Correlation between photoreactivity and charge-carrier recombination dynamics. *J. Phys. Chem.* **98,** 13669 (1994).
22. J.H. Chen, M.S. Yao, and X.L. Wang: Investigation of transition metal ion doping behaviors on TiO_2 nanoparticles. *J. Nano. Res.* **10,** 163 (2008).
23. A. Di Paola, E. Garcia-Lopez, S. Ikeda, G. Marci, B. Ohtani, and L. Palmisano: Photocatalytic degradation of organic compounds in aqueous systems by transition metal doped polycrystalline TiO_2. *Catal. Today* **75,** 87 (2002).
24. S.S. Srinivasan, J. Wade, E.K. Stefanakos, and Y. Goswami: Synergistic effects of sulfation and co-doping on the visible light photocatalysis of TiO_2. *J. Alloys Compd.* **424,** 322 (2006).
25. A. Ahmad, J.A. Shah, S. Buzby, and S.I. Shah: Structural effects of codoping of Nb and Sc in titanium dioxide nanoparticles. *Eur. J. Inorg. Chem.* 948 (2008).
26. H. Kato and A. Kudo: Visible-light-response and photocatalytic activities of TiO_2 and $SrTiO_3$ photocatalysts codoped with antimony and chromium. *J. Phys. Chem. B* **106,** 5029 (2002).
27. R. Niishiro, H. Kato, and A. Kudo: Nickel and either tantalum or niobium-codoped TiO_2 and $SrTiO_3$ photocatalysts with visible-light response for H_2 or O_2 evolution from aqueous solutions. *Phys. Chem. Chem. Phys.* **7,** 2241 (2005).
28. R. Niishiro, R. Konta, H. Kato, W.J. Chun, K. Asakura, and A. Kudo: Photocatalytic O_2 evolution of rhodium and antimony-codoped rutile-type TiO_2 under visible light irradiation. *J. Phys. Chem. C* **111,** 17420 (2007).
29. D.E. Huang, S.J. Liao, S.Q. Quan, L. Liu, Z.J. He, J.B. Wan, and W.B. Zhou: Preparation and characterization of anatase N-F-codoped TiO_2 sol and its photocatalytic degradation for formaldehyde. *J. Mater. Res.* **22,** 2389 (2007).
30. D. Li, H. Haneda, S. Hishita, and N. Ohashi: Visible-light-driven N-F-codoped TiO_2 photocatalysts. 1. Synthesis by spray pyrolysis and surface characterization. *Chem. Mater.* **17,** 2588 (2005).
31. J.G. Yu, M.H. Zhou, B. Cheng, and X.J. Zhao: Preparation, characterization and photocatalytic activity of in situ N,S-codoped TiO_2 powders. *J. Mol. Catal. A: Chem.* **246,** 176 (2006).
32. H.Y. Liu and L. Gao: (Sulfur,nitrogen)-codoped rutile-titanium dioxide as a visible-light-activated photocatalyst. *J. Am. Ceram. Soc.* **87,** 1582 (2004).
33. Y. Sakatani, H. Ando, K. Okusako, H. Koike, J. Nunoshige, T. Takata, J.N. Kondo, M. Hara, and K. Domen: Metal ion and N co-doped TiO_2 as a visible-light photocatalyst. *J. Mater. Res.* **19,** 2100 (2004).

34. Y. Sakatani, J. Nunoshige, H. Ando, K. Okusako, H. Koike, T. Takata, J.N. Kondo, M. Hara, and K. Domen: Photocatalytic decomposition of acetaldehyde under visible light irradiation over La^{3+} and N co-doped TiO_2. *Chem. Lett.* **32,** 1156 (2003).
35. C.C. Pan and J.C.S. Wu: Visible-light response Cr-doped $TiO_{2-x}N_x$ photocatalysts. *Mater. Chem. Phys.* **100,** 102 (2006).
36. S. Kim and S-K. Lee: Visible light-induced photocatalytic oxidation of 4-chlorophenol and dichloroacetate in intrided Pt-TiO_2 aqueous suspensions. *J. Photochem. Photobiol., A* **203,** 145 (2009).
37. Z.Y. Zhao and Q.J. Liu: Designed highly effective photocatalyst of anatase TiO_2 codoped with nitrogen and vanadium under visible-light irradiation using first-principles. *Catal. Lett.* **124,** 111 (2008).
38. Y. Wang, Y.L. Meng, H.M. Ding, Y.K. Shan, X. Zhao, and X.Z. Tang: A highly efficient visible-light-activated photocatalyst based on bismuth- and sulfur-codoped TiO_2. *J. Phys. Chem. C* **112,** 6620 (2008).
39. Z.Q. He, X. Xu, S. Song, L. Xie, J.J. Tu, J.M. Chen, and B. Yan: A visible light-driven titanium dioxide photocatalyst codoped with lanthanum and iodine: An application in the degradation of oxalic acid. *J. Phys. Chem. C* **112,** 16431 (2008).
40. R.D. Shannon: Revised effective ionic-radii and systematic studies of interatomic distances in halides and charcogenides. *Acta Crystallogr., Sect. A: Found. Crystallogr.* **32,** 751 (1976).
41. N. Serpone, D. Lawless, J. Disdier, and J.M. Herrmann: Spectroscopic, photoconductivity, and photocatalytic studies of TiO_2 colloid—Naked and with the lattice doped with Cr^{3+}, Fe^{3+}, and V^{5+} cations. *Langmuir* **10,** 643 (1994).
42. T. Umebayashi, T. Yamaki, H. Itoh, and K. Asai: Analysis of electronic structures of 3D transition metal-doped TiO_2 based on band calculations. *J. Phys. Chem. Solids* **63,** 1909 (2002).
43. A. Kudo, R. Niishiro, A. Iwase, and H. Kato: Effects of doping of metal cations on morphology, activity, and visible light response of photocatalysts. *Chem. Phys.* **339,** 104 (2007).
44. V.N. Kuznetsov and N. Serpone: Visible light absorption by various titanium dioxide specimens. *J. Phys. Chem. B* **110,** 25203 (2006).
45. N. Serpone: Is the band gap of pristine TiO_2 narrowed by anion- and cation-doping of titanium dioxide in second-generation photocatalysts? *J. Phys. Chem. B* **110,** 24287 (2006).
46. A.A. Lisachenko, V.N. Kuznetsov, M.N. Zakharov, and R.V. Mikhailov: The interaction of O_2, NO, and N_2O with surface defects of dispersed titanium dioxide. *Kinet. Catal.* **45,** 189 (2004).
47. V.N. Kuznetsov and T.K. Krutitskaya: Nature of color centers in reduced titanium dioxide. *Kinet. Catal.* **37,** 446 (1996).
48. R.A. Spurr and H. Myers: Quantitative analysis of anatase-rutile mixtures with an x-ray diffractometer. *Anal. Chem.* **29,** 760 (1957).